Journal of Pharmaceutical Sciences 110 (2021) 325-337

Contents lists available at ScienceDirect

Journal of Pharmaceutical Sciences

journal homepage: www.jpharmsci.org

Pharmacokinetics, Pharmacodynamics and Drug Transport and Metabolism

P-glycoprotein Substrate Assessment in Drug Discovery: Application of Modeling to Bridge Differential Protein Expression Across In Vitro Tools

Na Li [a], Priyanka Kulkarni [a], Akshay Badrinarayanan [a], Adey Kefelegn [a], Raffi Manoukian [b], Xingwen Li [a], Bhagwat Prasad [c], Matthew Karasu [c], William J. McCarty [a], Charles G. Knutson [a], Anshul Gupta [a, *]

[a] Department of Pharmacokinetics and Drug Metabolism, Amgen Research, Amgen Inc, Cambridge, MA 02142, USA
[b] Department of Cytometry Sciences, Amgen Research, Amgen Inc, Cambridge, MA 02142, USA
[c] Department of Pharmaceutical Sciences, Washington State University, Spokane, WA 99202, USA

ARTICLE INFO

Article history:
Received 2 July 2020
Revised 7 September 2020
Accepted 9 September 2020
Available online 15 September 2020

Keywords:
Drug transporter
P-glycoprotein
MDR1
P-gp expression
Kinetics
In vitro models
Efflux
Blood brain barrier
MDCK cells

ABSTRACT

P-glycoprotein (P-gp) efflux assay is an integral part of discovery screening, especially for drugs requiring brain penetration as P-gp efflux ratio (ER) inversely correlates with brain exposure. However, significant variability in P-gp ER generated across cell lines can lead to misclassification of a P-gp substrate and subsequently disconnect with brain exposure data. We hypothesized that the ER depends on P-gp protein expression level in the in vitro assay. Quantitative proteomics and immunofluorescence staining were utilized to characterize P-gp protein expression and localization in four recombinant cell lines, over-expressing human or mouse P-gp isoforms, followed by functional evaluation. Efflux data generated in each cell line was compared against available rodent brain distribution data. The results suggested that the cell line with highest P-gp expression (hMDCK-MDR1 sourced from NIH) led to greatest dynamic range for efflux; thus, proving to be the most sensitive model to predict brain penetration. Cell lines with lower P-gp expression exhibited the greatest tendency for compound-dependent in vitro efflux saturation leading to false negative results. Ultimately, P-gp kinetics were characterized using a compartmental model to generate system-independent parameters to resolve such discrepancy. This study highlights the need for careful choice of well characterized P-gp in vitro tools and utility of modeling techniques to enable appropriate interpretation of the data.

© 2020 American Pharmacists Association®. Published by Elsevier Inc. All rights reserved.

Introduction

Penetrating the blood-brain barrier (BBB) to achieve optimal target coverage at the site of action within the central nervous system (CNS) is the major hurdle for CNS drug discovery. The BBB consists of a continuous single layer of brain capillary endothelial cells with tight junctions, limiting the free exchange of xenobiotics between blood and CNS through paracellular penetration.[1,2] In addition, a diverse array of efflux pumps such as P-glycoprotein (P-gp) and Breast Cancer Resistance Protein (BCRP) are expressed along the BBB that attenuate the distribution of xenobiotics into the brain.[3–5]

The role of P-gp at BBB as a key determinant of CNS drug penetration has been widely established; compounds that are P-gp substrates exhibit poor brain penetration.[4,6] Thorough analysis of marketed CNS drugs and non-CNS drugs demonstrated a clear relationship between in vitro P-gp efflux and brain exposure measured in rodents.[6–8] Hence, an in vitro P-gp screening assay is an integral part of the early screening cascade, especially for CNS drug discovery programs, to triage molecules that are P-gp substrates.[9–11] Thus, development and validation of high fidelity P-gp transporter assay to determine P-gp substrate potential for new

Abbreviations: 3-C, 3-compartment; A, apical compartment; B, basolateral compartment; BBB, blood-brain barrier; BSA, bovine serum albumin; CNS, central nervous system; ER, efflux ratio; HBSS, Hank's balanced salt solution; IVIVE, in vitro to in vivo extrapolation; Kp_{uu}, Unbound partition coefficient; LC-MS/MS, liquid chromatography-tandem mass spectrometry; MDCK, Madin-Darby canine kidney; MDR1, multidrug resistance protein 1; NCE, new chemical entities; NIH, National Institute of Health; P-gp, P-glycoprotein.

Disclosure of Potential Conflicts of Interest: This study was funded by Amgen Inc, United States.
N.L., P.K., A.B., A.K., R.M., X.L., W.J.M., C.G.K., and A.G. are/were employees of Amgen at the time this work was performed, with stock interests or options in Amgen Inc. B.P. and M.K. have no potential conflict of interest to declare.

* Corresponding author. Department of Pharmacokinetics and Drug Metabolism, Amgen Research, Amgen Inc, 360 Binney Street, Cambridge, MA 02142.
E-mail address: agupta.pharmaceuticals@gmail.com (A. Gupta).

https://doi.org/10.1016/j.xphs.2020.09.017
0022-3549/© 2020 American Pharmacists Association®. Published by Elsevier Inc. All rights reserved.

chemical entities (NCEs) is critical in order to progress compounds with robust brain exposure in the clinic.

Human MDR1 overexpressed cell lines (MDCK or LLC-PK1 cells) are the most commonly used in vitro models to characterize P-gp substrate or inhibitor potential for NCEs. In vitro P-gp kinetic parameters can vary largely between laboratories because of differences in cellular systems and methodologies, thus reducing confidence in the data. Significantly large variability, as high as 796-fold, in IC_{50} values for P-gp inhibitors, was observed in an industry-wide study across 23 laboratories.[12] These differences were attributed to multiple factors including in vitro models (MDCK cell lines, LLC-PK cell lines and vesicles) utilized in this study. Similar observations have been made for substrate assessment where test concentration and cell line have been shown to be extremely critical.[13] The need for high analytical sensitivity combined with high K_m value reported for the classical P-gp substrates, has led researchers to employ 1 μM as the typical test concentration in P-gp efflux screening assay. However, recent shift in the chemical matter for discovery compounds has demonstrated unusual P-gp kinetic profiles based on our experience and others,[13] suggesting a Km value lower than 1 μM which may lead to saturation of P-gp mediated efflux at the standard test concentration (1 μM). Hence, in a single concentration screening assay under potentially saturating conditions, there is a high chance of misclassifying P-gp substrates. This makes identifying P-gp substrates, rank ordering lead molecules and progressing NCEs through the screening cascade, a significant challenge.

Further, it has been demonstrated that Michaelis-Menten kinetics may not work when estimating transport kinetics for ATP-binding cassette (ABC) transporters like P-gp.[14] This could be because the in vitro bidirectional cellular model used to characterize P-gp efflux is complex. It requires sophisticated modeling as the flux through multiple compartments in this model is dependent on the inherent permeability of the test compound. The 3-compartment, 5-compartment and structural mass action kinetic models have been proposed to characterize P-gp kinetics, which show less variable estimates of P-gp K_m values across different model systems.[15–19] Overall, identifying factors contributing to high variability in the in vitro P-gp assay/s and strategies that would allow to overcome such hurdles would significantly benefit drug discovery efforts.

In our laboratory, a disconnect was observed between in vitro P-gp efflux and in vivo rodent brain exposure data. This correlation seemed to vary depending on the choice of cell line. We hypothesized that P-gp protein expression differences across the in vitro models, is largely responsible for this discrepancy. To address this question, we conducted a systematic characterization of four different P-gp overexpressing cell lines; human MDR1-MDCKII and murine Mdr1a-MDCKII cell lines generated using Flp-In™ System, human MDR1-MDCK cell line in-licensed from National Institutes of Health (NIH), and ready-to-use human MDR1-MDCKII cells procured from external vendor. Cell lines engineered with the same commonly used background strain, i.e. MDCK, were utilized in this analysis to avoid confounding factors related to the inherent differences of parental cell lines, influencing the results. Murine mdr1a over-expressing MDCK cell line was also included to address questions related to species dependent substrate specificity.

To confirm protein expression differences, P-gp was quantified using targeted proteomics while cellular localization was evaluated using confocal microscopy. A set of proprietary compounds from our neuroscience discovery portfolio was selected to assess the predictability of brain exposure from the in vitro P-gp transporter assay. Finally, compartment modeling approach was applied to determine P-gp kinetics and obtain system-independent K_m values in an effort to bridge the gap across these in vitro models and to resolve IVIVE disconnect.

Materials and Methods

Chemicals and Reagents

A set of 48 proprietary compounds used in this study were selected from neuroscience discovery programs at Amgen. These compounds were selected based on the in vitro to in vivo disconnect observed in brain penetration data. Additionally, compounds I-VI were selected as representative molecules to highlight differential P-gp saturation and perform kinetic modeling, where appropriate. All compounds were obtained from the Amgen Sample Bank (Thousand Oaks, CA). Dulbecco's Modified Eagle Medium (DMEM) with Glutamax and 4.5 g/L glucose, Non-Essential Amino Acids (NEAA), 100× sodium pyruvate and Hygromycin B were obtained from Thermo Fisher Scientific (Waltham, MA). Fetal bovine serum (FBS) was purchased from Corning Life Sciences (Tewksbury, MA). Dimethyl sulfoxide, colchicine and 4% formaldehyde were purchased from MilliporeSigma (St. Louis, MO). HPLC grade acetonitrile and water were purchased from Burdick & Jackson (Muskegon, MI).

Cell Culture and Maintenance

The human MDR1 and murine Mdr1a transfected MDCKII, designated as hMDR1-MDCKII and mMdr1a-MDCKII, and vector control transfected MDCKII cell lines were engineered using Flp-In™ System (Thermo Fisher Scientific) and maintained in DMEM (1×) (with Glutamax, 4.5 g/dL glucose) containing 10% FBS, 1 mM sodium pyruvate and 0.1 mM NEAA supplemented with selection agent hygromycin B (100 μg/mL). The well-established human MDR1 overexpressing MDCK cell line (NIH hMDR1-MDCK) commonly used across industry, was procured from NIH (Bethesda, MD). These cells were maintained in DMEM (1×) (with Glutamax, 4.5 g/dL glucose) containing 10% FBS, 1 mM sodium pyruvate and 80 ng/mL colchicine. The ready-to-use 96-well TransFlex™ plate containing MDCKII Cells stably expressing human MDR1 protein were purchased from Optivia Biotechnology, BioIVT (Santa Clara, CA). All cell lines were grown at 37 °C, 5% CO_2 and 95% humidity.

P-gp Protein Quantification Using Targeted Proteomics

P-gp protein quantification was carried out using LC-MS/MS proteomics method.[20] A surrogate peptide was selected for P-gp, EIIGVVSQEPVLFATTIAENIR (amino acid residues from 468 to 489), which is located at the sixth cytoplasmic loop.[2] The total membrane protein extracted from pellets obtained from each cell line[21] was denatured, reduced, alkylated as per published protocol.[20] Similarly, the denatured/alkylated protein was then desalted and precipitated using methanol: chloroform: water precipitation followed by tryptic digestion as described before.[20] The digestion reaction was quenched by 20 μL of labeled peptide internal standard cocktail containing the heavy labeled peptide (EIIGVVSQEPVLFATTIAENIR [^{13}C and ^{15}N]) plus 10 μL of blank solvent (50% acetonitrile in water containing 0.1% formic acid). The samples were centrifuged and injected onto the LC-MS/MS system as described previously.[21] Briefly, samples were analyzed using an Acquity UPLC (M Class) coupled with Xevo TQ XS (Ion Key interface) (Waters, Milford, MA). iKey BEH C18 column (130 A°,1.7 μm, 150 μm × 50 mm) and nano Ease Symmetry C18 trap column (300 μm × 50 mm) (Waters, Milford, MA) was used to achieve chromatographic peptide separation. The LC and MS parameters used for the quantification are provided in Supplementary Table 1S. Skyline software (University of Washington, Seattle, WA) was used to process acquired data.

The dynamic range of peptide quantification was established by performing analysis of the serial dilutions of the heavy peptides (concentration equivalent to ~0.1-fold lower and 100-fold higher of the light response). The absolute quantification of the surrogate peptide was performed by using a single point calibration approach, where a pooled total membrane sample isolated from liver tissue with known transporter abundance was used as the calibrator.

Bidirectional P-gp Efflux Transport Assay

Based on previously optimized assay conditions for each cell line, hMDR1-MDCKII and mMdr1a-MDCKII were seeded at a density of 1×10^5 cells/well and NIH hMDR1-MDCK cells were seeded at a density of 0.5×10^5 cells/well in a 96-well Millicell® insert plates (EMD Millipore) with selection agent free media and maintained at 37 °C, 5% CO_2 and 95% humidity for 5 days. Fresh seeding media was added to the plates on the third day and transport experiments were carried out on the fifth day. The ready-to-use 96-well TransFlex™ hMDR1-MDCKII cell plates were used in accordance with the manufacturer's recommended procedure.

All bidirectional efflux assays using MDCK cell line were fully validated. Briefly, these were carried out using HBSS (1× with calcium and magnesium) containing 10 mM HEPES at pH 7.4 and 0.1% BSA. Prior to running the experiment, the media was aspirated, and the cells were washed thrice with assay buffer. A 96-well Millicell® feeder/receiver tray (EMD Millipore) was used for basolateral dosing and collection. Test articles were dosed in the apical chamber when measuring A to B permeability and in the basolateral chamber when measuring B to A permeability. The monolayer integrity, positive control and recovery are routinely measured in every experiment to ensure the data integrity. Labetalol and prazosin were used as positive controls for strong and moderate P-gp substrates, respectively. Atenolol was used as cell monolayer integrity marker or low permeability control. The assay was conducted at triplicate for controls and test compounds. The data for the test compounds were only reported when all the data for the controls fell within the acceptable range and the CV% of the triplicate is less than 20%. After 2-hrs incubation at 37 °C, the samples were collected from donor and receiver for LC-MS/MS analysis. The dosing solutions were used to calculate the recoveries post-assay. The apparent permeability (P_{app}) was calculated with the following equation,

$$Papp = \frac{dQ}{dt}\left(\frac{1}{A \times C0}\right)$$

Where dQ/dt is the apical-to-basal penetration rate of the compound, A is the surface area of the cell monolayer on the insert filter membrane, and C_0 is the initial concentration of the test compound. Efflux ratio (ER) was calculated with the following equation,

$$ER = \frac{Papp_{B \to A}}{Papp_{A \to B}}$$

Where, Papp $_{A \to B}$ is the apparent permeability in A to B direction, Papp $_{B \to A}$ is the apparent permeability in the B to A direction.

LC-MS/MS Quantification

The samples from transport studies were analyzed using a triple quadruple mass spectrometer (Triple Quad 5500, AB Sciex, Framingham, MA) coupled to a Shimadzu Nexera XR/X2 UPLC system. The mass spectrometer was operated with positive electrospray ionization mode with a source voltage of 5000 V and temperature of 500 °C. Automated MRM (Multiple Reaction Monitoring) method optimization and quantitative analysis were performed using the integrated DiscoveryQuant software (version 3.0.1, Sciex). A sample volume of 5 μL was injected using a Shimadzu SIL30ACMP temperature controlled autosampler. Analytes were separated using a Cadenza CD-C18 (Imtakt Corp., 30 mm × 2 mm, 5 μm) analytical column maintained at 40 °C. The mobile phase consisted of water with 0.1% formic acid as solvent A and acetonitrile with 0.1% formic acid as solvent B. The flow rate was set at 1.5 mL/min and the total run time for each sample injection was 1 min. The elution gradient started with 1% solvent B until 0.15 min where solvent B was held at 10% until 0.25 min. Between 0.25 min and 0.75 min, solvent B was decreased back to 1% and allowed to equilibrate until 1 min.

Immunofluorescence Staining and Confocal Imaging

The hMDR1-MDCKII and NIH hMDR1-MDCK cells were seeded in a 96well black-walled plate with optical grade glass bottom (PerkinElmer, Waltham, MA) due to incompatibility of transwell plates with confocal microscope. These plates were maintained at 37 °C, 5% CO_2 and 95% humidity for 3 days. The cell monolayers were then rinsed with phosphate-buffered saline (PBS) and fixed with 10% neutral buffered formalin (4% formaldehyde v/v) for 20 min. The fixed monolayers were permeabilized with 0.1% Triton X-100 solution for 20 min. The samples were then incubated with anti-human P-gp monoclonal antibody Clone#MRK16 (Enzo life sciences, Farmingdale, NY) overnight at 4 °C, followed by incubation with goat anti-mouse IgG cross-adsorbed secondary antibody conjugated with Alexa Flour® 647 (Jackson ImmunoResearch Laboratories, West Grove, PA) for 2 h at room temperature. Cells were washed and overlaid with buffer containing 2 μg/ml of DNA intercalating dye, Hoechst 33342 (ThermoFisher).

High-content imaging was performed on a PerkinElmer Ultraview Vox, dual spinning-disc confocal microscope (PerkinElmer, Waltham, MA, USA) using laser excitation wavelengths of 405 nm and 633 nm. The microscope consists of an inverted stage with a sample holder that accommodates the above-mentioned plates allowing for high resolution imaging through the bottom of the plate well. Nikon Plan Fluor 20×/0.75 and Apo TIRF 60×/1.49 oil objectives were used for image acquisition. Single plane optical slice images were taken and represent a thickness of approximately 0.5 μM with the 20× magnification objective and 0.15 μM with the 60× magnification objective. Using the 60× oil objective, approximately 30 optical slices were sequentially imaged to create a confocal z-stack which could be viewed as a maximum projection, an orthogonal cross-sectional view (xy, xz, yz), or a 3-D rendered image. Images were acquired and analyzed using Volocity software 6.3 (PerkinElmer). All instrument exposure times and laser power settings were kept constant between samples to allow for inter-sample comparison.

Kinetic Modeling of P-gp Mediated Efflux

The P-gp kinetic assay was performed for quinidine using hMDR1-MDCKII cells, and for Amgen proprietary compounds, designated as compound IV and compound V using the TransFlex™ hMDR1-MDCKII cell line, at a range of concentrations. The 3-Compartment (3-C) model as shown in Fig. 6A was applied to characterize the P-gp kinetics by analyzing the bidirectional transport data. The 3-C model was simultaneously fit to receiver and donor concentrations for both apical-to-basolateral and basolateral-to-apical directions measured at 1.5-hrs for Quinidine and at 2-hrs for Compounds IV and V. The V_{max} and K_m of P-gp, passive diffusion clearance (CL_d) and $f_{u,cell}$ were parameterized. Back diffusion from the receiver compartments due to passive

diffusion was explicitly modeled. Hence, no assumptions regarding maintaining linearity or reaching steady-state were necessary. For all the experiments conducted using TransFlex™ hMDR1-MDCKII, the volume of apical (Va) and basolateral (Vb) compartments were fixed to the experimental volumes of 100 and 300 μL, respectively. The cell volume (Vc) was scaled from Korzekwa et al. proportional to the insert surface area of 0.27 cm^2 and fixed to 0.482 μL assuming a monolayer of cells.[22] For all experiments conducted using hMDR1-MDCKII and NIH hMDR1-MDCK, Va and Vb were fixed to the experimental volumes of 60 and 180 μL, respectively. The Vc for In-house and NIH cells was scaled from Korzekwa et al. proportional to the insert surface area of 0.11 cm^2 and fixed to 0.196 μL assuming a monolayer of cells.[22] In all modeling exercises, the fraction unbound in the incubation medium containing 0.1% BSA was fixed to 0.746, 0.183 and 0.57 respectively, for Quinidine, Compound IV and Compound V which was measured using ultracentrifugation method as previously described with slight modification.[23]

To assess the system independence of the K_m and estimate the ratio of surface-active P-gp from different MDR1 cell lines, the P-gp efflux of compound IV and V were experimentally determined at range of concentration of 0.1 μM, 1 μM and 5 μM in hMDR1-MDCKII and NIH hMDR1-MDCK cell line respectively. Subsequently, the 3-C model was fit to these data with fixed K_m obtained from the compartmental modeling as described above, and passive diffusion (CL_d), along with R1 (TransFlex™ hMDR1-MDCKII versus hMDR1-MDCKII) for hMDR1-MDCKII or R2 (TransFlex™ hMDR1-MDCKII versus NIH MDR1-MDCKII) for NIH MDR1-MDCKII were parameterized. Passive diffusion along the concentration gradient across a cell monolayer can occur either through the cells (transcellular) or in between the cells (paracellular).[24–26] The current model did not separately account for transcellular and paracellular passive permeability. Hence, the combined passive diffusion term, CL_d, was also parameterized in this study.

Quantitative targeted proteomics provided the total membrane P-gp content in the cells and it was evident from the immunofluorescence and confocal microscopy studies that significant P-gp was localized in the hMDR1-MDCK cells, thus preventing clear quantitative information regarding the surface expression level of P-gp. To maintain consistency in the modeling approach used for both the cell lines, we did not use the experimentally determined P-gp expression level in the model. Instead, the V_{max} was used as an indication of protein expression differences. As more sophisticated analytical approaches to precisely measure plasma membrane associated active transporter protein become available, the modeling techniques can evolve to incorporate these details. Wolfram Mathematica (Version 11.2) was used for modeling and simulation. The NDSolve function in Mathematica with AccuracyGoal → 10, PrecisionGoal → 10, MaxSteps → 1,00,000 was used to obtain numeric solutions of the ordinary differential equations. The NonlinearModelFit function was used for parameter estimation.

Statistical Analysis

GraphPad Prism (Version 8.3.0) was used for statistical analysis of the experimental data. Targeted proteomic P-gp expression was compared across groups using a one-way ANOVA and Tukey post-hoc tests (Fig. 1). Pearson's correlation coefficients were calculated to understand the relationship between P-gp ERs generated across cell lines (Fig. 2). An ANCOVA was used to assess whether the mouse Kpuu vs. P-gp ER relationships were different across the cell lines (Fig. 3). P-values < 0.05 were considered significant.

Results

Characterization of P-gp Protein Expression in Various P-gp Overexpressing Cell Lines

Targeted proteomics using LC-MS/MS to quantitatively determine the abundance of enzymes and transporter proteins to facilitate IVIVE has been reported previously.[27,28] The abundance of P-gp protein was quantified using surrogate peptide-based LC-MS/MS proteomics in four established P-gp cell lines transfected with either human MDR1 (referred to as hMDR1-MDCKII, NIH hMDR1-MDCK and TransFlex™ hMDR1-MDCKII) or mouse mdr1a (mMdr1a-MDCKII) that are commonly used across industry. In addition, MDCKII transfected with vector control were utilized as negative control to determine the baseline or canine P-gp expression. For LC-MS/MS analysis, the chosen surrogate peptide represented the fragment cleaved from tryptic proteolysis of P-gp and was conserved across species.[2] The amount of P-gp in each cell line, expressed as pmol per mg of total membrane protein (Fig. 1A), indicated that P-gp expression varied significantly across cell lines (ANOVA, $p < 0.01$) with the following rank order: NIH hMDR1-MDCK > mMdr1a-MDCKII > TransFlex™ hMDR1-MDCKII > hMDR1-MDCKII. Statistically significant differences were found between the hMDR1-MDCKII vs. mMdr1a-MDCKII ($p < 0.01$), hMDR1-MDCKII vs. NIH hMDR1-MDCK ($p < 0.001$), mMdr1a-MDCKII vs. TransFlex™ hMDR1-MDCKII ($p < 0.01$), and NIH hMDR1-MDCK vs. TransFlex™ hMDR1-MDCKII ($p < 0.001$) cell lines. Although vector control-MDCKII cells are expected to express endogenous P-gp, the level of canine P-gp protein was determined to be below the lower limit of quantification (1.7 pmol/mg protein) in our studies (data not shown).

P-gp is a transmembrane protein with multiple transmembrane domains and only the functional protein expressed on the cell surface is responsible for its efflux activity. Therefore, confocal microscopy was used to investigate the P-gp expression and localization in two of the four human P-gp cell lines monolayer, i.e., hMDR1-MDCKII with lowest P-gp level and NIH hMDR1-MDCK with highest P-gp level. Due to the incompatibility of transwell assay plates for imaging under confocal microscopy, black wall optical plates were used assuming no change in the morphology of cell monolayers as well as P-gp expression and localization based on internal observation. The cells were stained with Hoechst dye which highlighted spherical and evenly distributed nuclei (in blue), while P-gp was visualized by indirect immunofluorescence (in red) (Fig. 1C). Based on XY magnification and front-view, it is evident that P-gp expression in NIH hMDR1-MDCK monolayer was much more pronounced as compared to hMDR1-MDCKII (Fig. 1C), which aligned with the P-gp abundance data as determined by targeted proteomics. Interestingly, P-gp was localized exclusively on the apical membrane of the NIH hMDR1-MDCK monolayer versus hMDR1-MDCKII where significant portion of P-gp staining was found in cytoplasm based on the orthogonal view (Fig. 1C, b and d) as well as confocal z stack 3D images (Fig. 1C, e and f). Additionally, these two cell lines demonstrated dramatic morphological differences; hMDR1-MDCKII cells exhibited characteristic polygonal shape, while NIH hMDR1-MDCK cells exhibited elongated spindle shape. The results are consistent with the condition when the cells are grown on filter inserts (data not shown).

Comparison of Functional Activity Between hMDR1-MDCKII, mMdr1a-MDCKII and NIH hMDR1-MDCK Cell Lines

The NIH hMDR1-MDCK showed the highest P-gp activity (ER) for the positive control substrates, prazosin and labetalol, followed by mMdr1a-MDCKII, while hMDR1-MDCKII showed the lowest

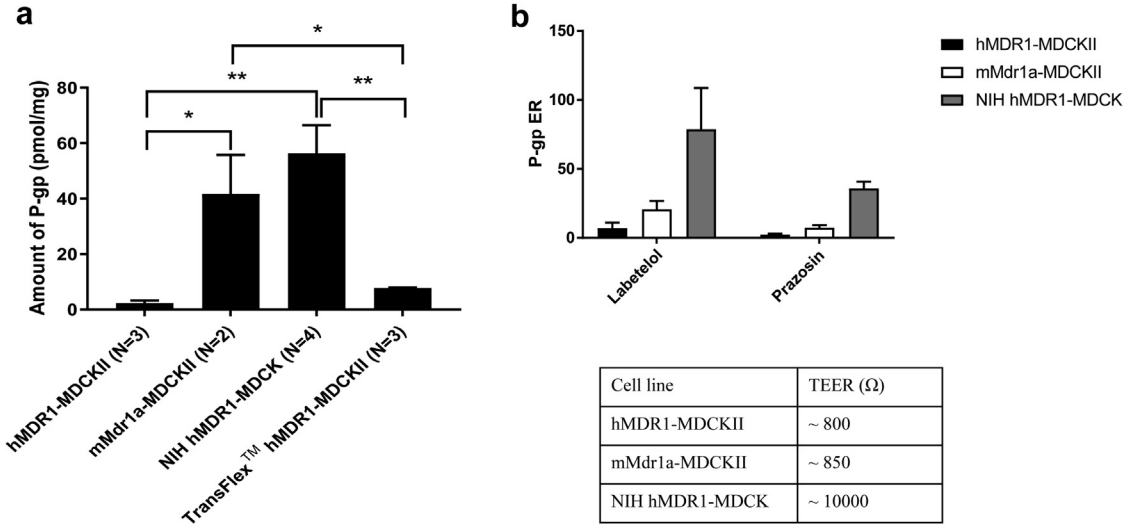

Cell line	TEER (Ω)
hMDR1-MDCKII	~ 800
mMdr1a-MDCKII	~ 850
NIH hMDR1-MDCK	~ 10000

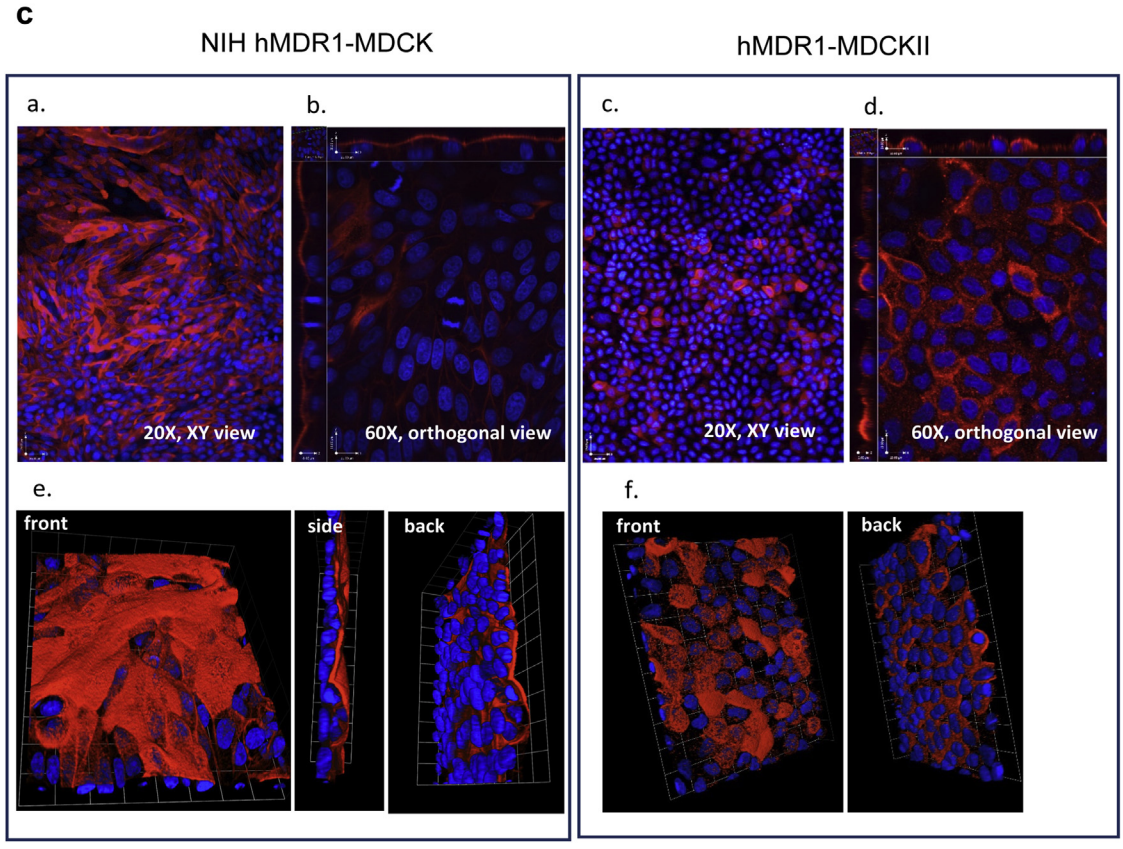

Fig. 1. Characterization of P-gp expression and localization in P-gp over-expressing cell lines. (A) Targeted proteomics analysis of hMDR1-MDCKII, mMdr1a-MDCKII, NIH hMDR1-MDCK and TransFlex™ hMDR1-MDCKII cell lines. Data represents the mean P-gp expression level + S.D. (n = 2–4 as indicated in the graph). Tukey post-hoc analysis showed significant differences in expression between the groups: *$p < 0.01$ and **$p < 0.001$. (B) The comparison of efflux ratios of two P-gp substrates between hMDR1-MDCKII, mMdr1a-MDCKII and NIH hMDR1-MDCK. Data represents mean + S.D. (n = 5–7). Transepithelial electrical resistance (TEER) measurements were also determined in these three cell lines as indicated. (C) P-gp expression and localization in the NIH hMDR1-MDCK and hMDR1-MDCKII cell lines using immunofluorescence and confocal imaging. Based on 20×, XY view, evenly spread high level of P-gp expression was observed in NIH hMDR1-MDCK cells (a), whereas hMDR1-MDCKII cells had significantly lower levels expressed heterogeneously (c). An orthogonal representation of a z-stack image at 60× oil magnification, where the x,y plane represents a cross-section midway through the cellular field, demonstrates complete cell surface localization of P-gp in NIH hMDR1-MDCK (b) versus P-gp expression on both cell surface and intracellular compartment for hMDR1-MDCKII (d). Furthermore, through a 360° view of the cell monolayer via 3-D rendering of the z-stacks, P-gp staining was exclusively localized on the apical membrane of NIH hMDR1-MDCK cell monolayer with no intracellular signal (e). However, P-gp staining in hMDR-MDCKII cell monolayer was localized both on the cell surface as well as intracellularly (f).

activity (ER) (Fig. 1B), which aligns well with the P-gp expression level in the corresponding cell lines. The specificity of P-gp function was further verified in NIH hMDR1-MDCK cell line using a list of CNS targeted and non-CNS targeted drugs. In general, P-gp ER generated in the NIH hMDR1-MDCK cell line in our lab was in good agreement with that observed by other groups[29] and correlated well with the brain penetration in rodent (Supplemental Table S2).[30] In addition, NIH hMDR1-MDCK cell line

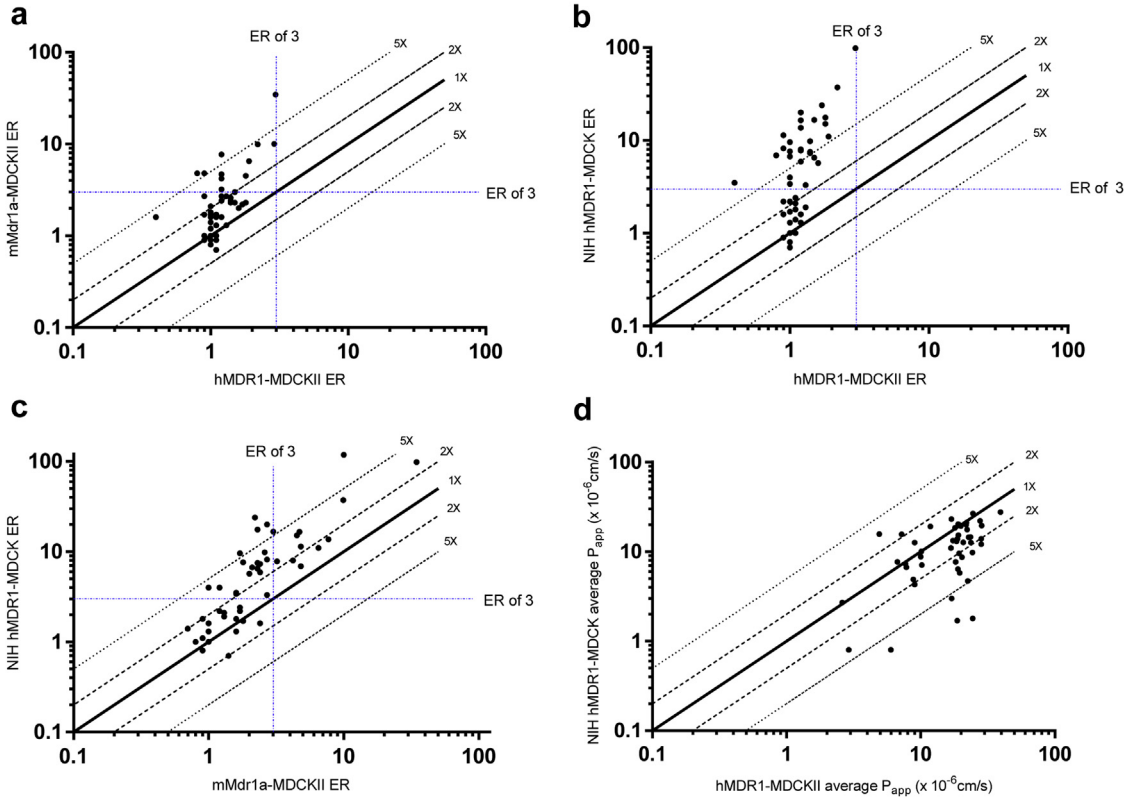

Fig. 2. P-gp efflux ratios across the three cells lines for a set of compounds selected from CNS discovery programs were positively correlated (Pearson's r): (A) hMDR1-MDCKII vs mMdr1a-MDCKII (r: 0.72, $p < 0.001$); (B) hMDR1-MDCKII vs NIH hMDR1-MDCK (r: 0.85, $p < 0.001$); (C) mMdr1a-MDCKII vs NIH hMDR1-MDCK (r: 0.78, $p < 0.001$). ER of 3 are used as the cutoff to classify P-gp substrates. (D) The average permeability determined in hMDR1-MDCKII of this set of compounds was compared with those determined in NIH hMDR1-MDCK cells. The solid, dashed and dotted lines represent the line of unity, 2-fold and 5-fold difference.

demonstrated much higher TEER value compared to hMDR1 MDCKII and mMdr1a MDCKII cells (Fig. 1B). The performance of each cell line for rank ordering or binning of discovery molecules based on P-gp functional activity was evaluated by testing a set of 48 compounds from neuroscience discovery projects where P-gp was believed to be the major determinant of brain penetration and corresponding brain partitioning data in rodents were available. While the P-gp ER calculated for this set of compounds across cell lines were positively correlated (Pearson's r, p-value): hMDR1-MDCKII vs mMdr1a-MDCKII (r: 0.72, $p < 0.001$); hMDR1-MDCKII vs NIH hMDR1-MDCK (r: 0.85, $p < 0.001$); mMdr1a-MDCKII vs NIH hMDR1-MDCK (r: 0.78, $p < 0.001$), differences in dynamic range were apparent (Fig. 2). An arbitrary ER cut-off value of 3 is typically used for P-gp screening assay in discovery to bin compounds such that any test compound with an ER > 3 is determined to be a P-gp substrate. Following these criteria, none of the selected 48 compounds were identified as P-gp substrates using hMDR1-MDCKII. In addition, the efflux in parental MDCK cell line for 34 out of 48 compounds were close to unity (Supplemental Table S3). However, 12 out of 48 compounds were identified as P-gp substrates when using mMdr1a-MDCKII (Fig. 2A); 30 out of 48 compounds were identified as P-gp substrates when using NIH hMDR1-MDCK (Fig. 2B). Although the P-gp ER of mMdr1a-MDCKII and NIH hMDR1-MDCK cell lines were correlated (Fig. 2C), the latter cell line exhibited a greater dynamic range which can be explained by its higher P-gp expression. There was no statistically significant difference in the average P_{app} determined between hMDR1-MDCKII and mMdr1a-MDCKII (data not shown); however, the average P_{app} determined in NIH hMDR1-MDCK cell line was significantly lower than those determined in hMDR1-MDCKII (Fig. 2D). This may be explained by the higher TEER values in NIH hMDR1-MDCK compared to the other two cell lines made from parental MDCKII cell line (Fig. 1B).

Subsequently, the P-gp ER determined in these three cell lines were evaluated against the corresponding brain exposure data in rodents (brain Kp_{uu} determined by the ratio of unbound brain concentration versus the unbound plasma concentration) (Fig. 3) that was available in the Amgen database. The best-fit lines through the mouse Kpuu vs. P-gp ER data were significantly different between cell lines (ANCOVA, $p < 0.0001$). The P-gp ER of 3 and brain Kp_{uu} of 0.3 were used as cut-offs to classify the compounds into four quadrants based on the prediction performance for brain penetration (Q1: true positive; Q2: false negative; Q3: false positive; Q4: true negative). The predictability of the three P-gp cell lines are summarized in Fig. 3D. When hMDR1-MDCKII was used to assess the P-gp efflux, 80% (38 out of 48) of the compounds fell into Q3 where the compounds characterized as P-gp non-substrates showed poor brain penetration (Fig. 3A). The P-gp activity determined using NIH hMDR1-MDCK greatly improved the relationship between ER and brain Kp_{uu} as majority of the compounds fell into upper left (Q1) and bottom right (Q4) (Fig. 3B). A few compounds (3 out of 10) shifted to upper right quadrant (Q2) where the compounds which appear as P-gp substrates showed favorable brain exposure (Fig. 3B), suggesting the possible involvement of active uptake transporter for brain uptake of these compounds. Murine Mdr1a-MDCKII improved the correlation of P-gp ER with brain exposure, but to lesser extent compared to the NIH cell line (Fig. 3C). These data suggest that P-gp expression levels are critical for the performance of cell lines for evaluation of test articles, i.e. the cell lines with higher P-gp expression demonstrated higher P-

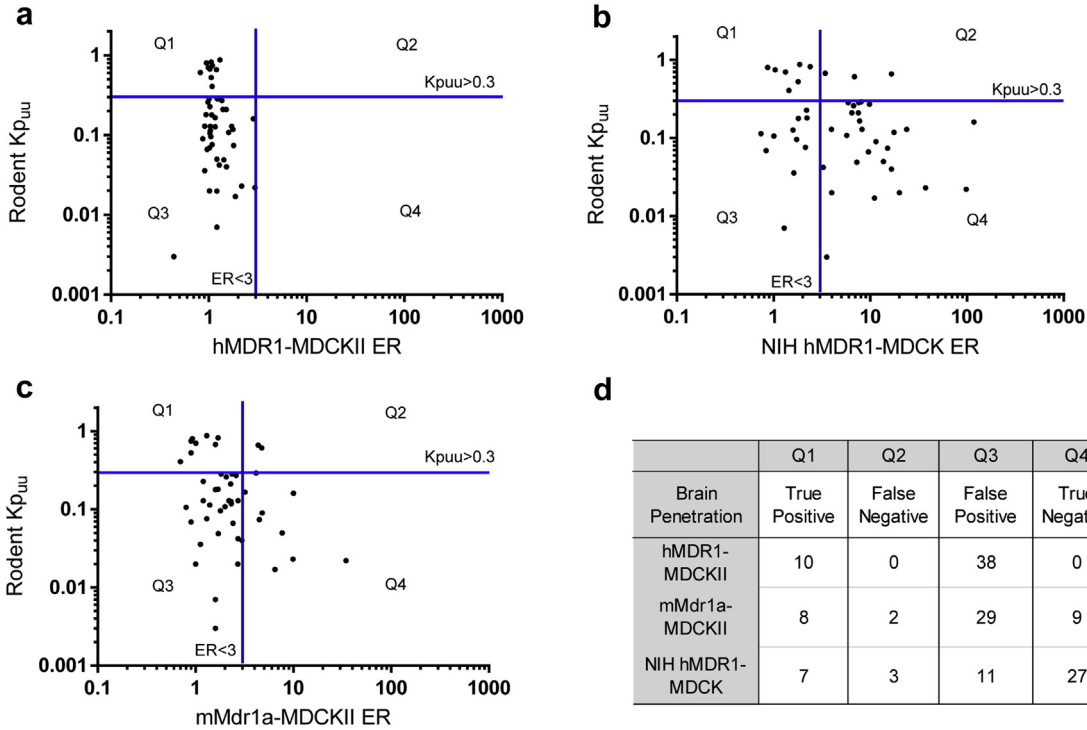

	Q1	Q2	Q3	Q4
Brain Penetration	True Positive	False Negative	False Positive	True Negative
hMDR1-MDCKII	10	0	38	0
mMdr1a-MDCKII	8	2	29	9
NIH hMDR1-MDCK	7	3	11	27

Fig. 3. Correlation of brain penetration data in rodents with P-gp efflux ratios generated using in hMDR1-MDCKII (A); NIH hMDR1-MDCK (B); and mMdr1a-MDCKII (C). Brain penetration was assessed by brain Kp_{uu} ($C_{b,u}/C_{p,u}$) in rodent. ER of 3 and Kp_{uu} of 0.3 were used as the cutoff for P-gp substrates and for brain penetrant respectively. The best-fit lines through the mouse Kpuu vs. P-gp ER data were significantly different between cell lines (ANCOVA, $p < 0.0001$). The graph was divided into four quadrants, Q1 is upper left, Q2 is upper right, Q3 is bottom left and Q4 is bottom right. (D) The number of compounds in each quadrant were summarized for each P-gp cell line, which was used to access the predictability of brain penetration.

gp efflux and greater dynamic range to distinguish P-gp substrates from non-substrates, leading to better prediction of brain penetration.

P-gp Saturation in hMDR1-MDCKII Versus NIH hMDR1-MDCK

One of the potential reasons for discrepancy in ER values across cell lines is P-gp saturation at test concentration which depends on compound specific kinetic parameters related to P-gp expression in each cell line. To study this hypothesis, concentration-dependent P-gp efflux was conducted for a series of compounds (labeled I– VI) selected from neuroscience discovery projects in hMDR1-MDCKII and NIH hMDR1-MDCK (Fig. 4). For P-gp substrates, under non-saturating conditions (low donor concentration), it is expected that the apparent P_{app} A to B is lowest and apparent P_{app} B to A is highest leading to highest ER value as P-gp function is in full capacity. With an increase in donor concentration, P-gp can gradually saturate resulting in an increased P_{app} A to B and a decreased P_{app} B to A. At a certain concentration where P-gp is fully saturated, P_{app} A to B and P_{app} B to A reach a plateau and the ER approaches unity. In hMDR1-MDCKII, P-gp activity of compound I, II, III and IV, was highest at 0.1 μM followed by 1.0 μM and fully saturated at 5 μM. However, P-gp ER for compound V and VI at 1 μM was 1.4 and 1.1, respectively suggesting saturation (Fig. 4). Although, these compounds would be classified as P-gp non-substrates if only tested at1 μM. In contrast, P-gp capacity was markedly higher in NIH hMDR1-MDCK cell line as compared to hMDR1-MDCKII. At the lowest test concentration of 0.1 μM, ER values were significantly higher for all test compounds in the NIH hMDR1-MDCK cell line compared to hMDR1-MDCKII. No significant difference was observed in the ER values when tested at 0.1 and 1 μM for each of the compounds suggesting no saturation. At 5 μM test concentration, four compounds (I, IV, V and VI) demonstrated saturation, but not compound II and III (Fig. 4).

Estimation of P-gp Kinetics Using 3-C Model

To explore the system-independent P-gp kinetic parameters, three compartment (3-C) model (Fig. 5A) was used for the select compounds (IV and V) and P-gp model substrate, quinidine. These results are summarized in Table 1. The model predicted and observed concentrations from donor and receiver compartment from the bidirectional transport of quinidine using hMDR1-MDCKII and compounds IV and V using TransFlex™ hMDR1-MDCKII are shown in Fig. 5B. Overall, the 3-C model well predicted the receiver and donor concentrations from the bidirectional transport assay with the adjusted R^2 of 0.924, 0.988 and 0.97 for quinidine, compounds V and IV, respectively. The estimated K_m for quinidine was 0.26 μM which is comparable to the literature reported K_m from compartmental modeling (0.19–0.34 μM),[15,16] hence further validating the compartmental modeling approach for consistently estimating the system-independent 'true' kinetic parameters of P-gp substrates.

By fixing the K_m determined above, the P-gp efflux in hMDR1-MDCKII and NIH hMDR1-MDCK was simulated and compared with the experimentally determined data (Fig. 6). In addition, the surface-active P-gp ratio was determined by simulation (Table 1). The data showed that surface-active P-gp protein in hMDR1-MDCKII cell line was 0.22–0.33-fold of that in TransFlex™ hMDR1-MDCKII cell line. While, the surface-active P-gp protein in NIH hMDR1-MDCK cell line was 1.24–1.59-fold of that in TransFlex™ hMDR1-MDCKII. It is important to note that upon accounting for difference in surface-active P-gp and the inter-day and inter-system differences in passive diffusion (estimated CL_d), the system-

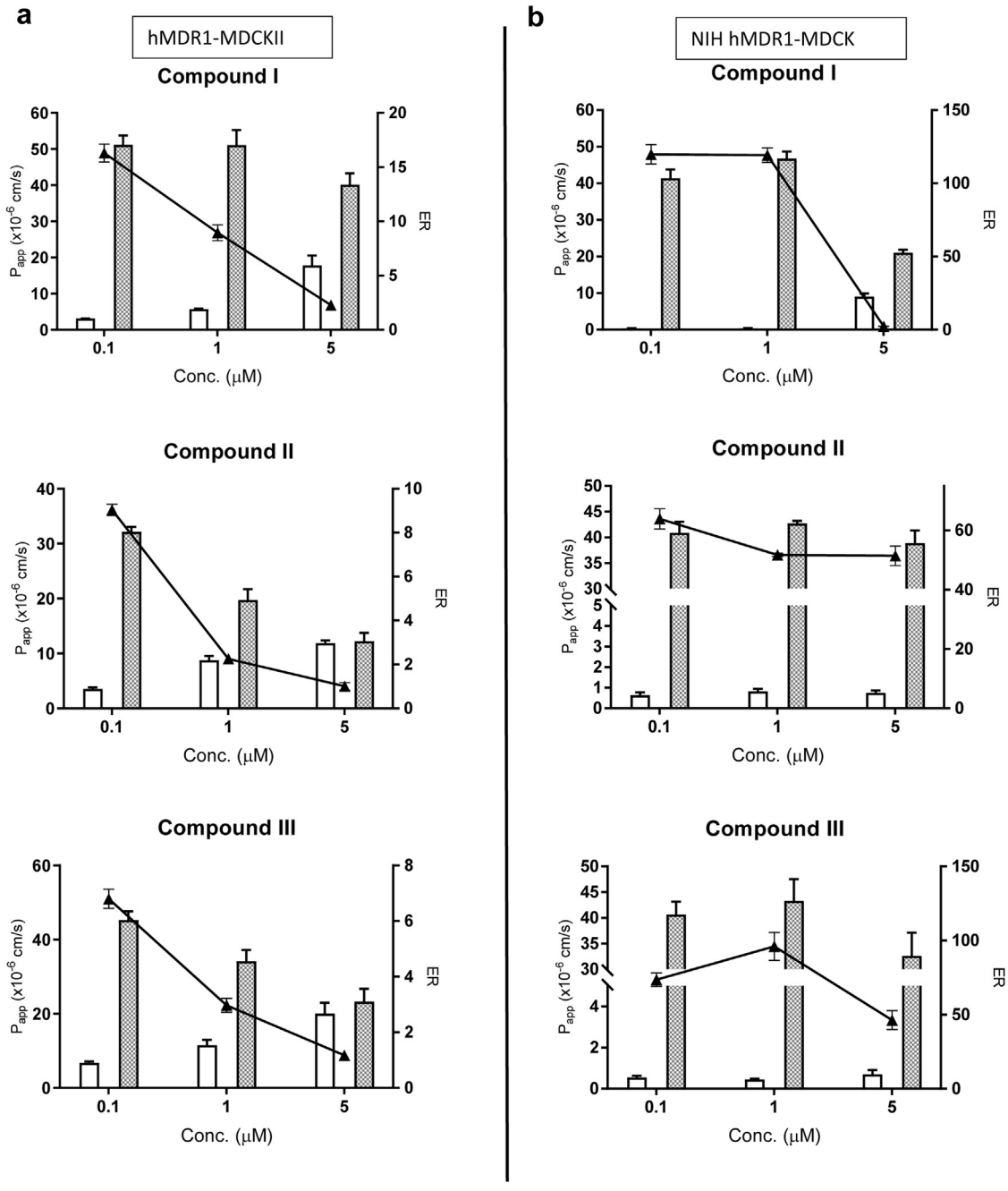

Fig. 4. Concentration-dependent P-gp efflux in hMDR1-MDCKII (A) and NIH hMDR1-MDCK cell lines (B). P-gp efflux of compound I, II, III, IV, V and VI were determined at concentration of 0.1 μM, 1.0 μM and 5.0 μM at 2-hrs incubation in hMDR1-MDCKII and NIH hMDR1-MDCK cell monolayers respectively. Open bar represents $P_{app\ A>B}$; Patterned bar represents $P_{app\ B>A}$ and solid triangle represents P-gp ER at indicated concentration. Data represents mean of triplicate measurements with SD.

independent 'true' K_m was able to predict the experimentally observed concentrations, the permeability and efflux ratios in the bidirectional transport experiments for compounds IV and V in different MDR1 cell lines (Fig. 6).

It was noted that P-gp ER was affected by the P-gp expression level in different cell lines for some compounds, but not for others. Fig. 7 demonstrates the simulated effect of differential P-gp expression level on P-gp ER (A) and fold change in ER (B) at a range of K_m values. The results suggested that the higher the expression level of P-gp, higher the P-gp ER although depending on the "true" Km value, the values between the two systems can converge. It is important to note that the extent of change in ER between systems with varying protein expression, is more prominent for compounds with lower K_m values; and this ER fold-change gets smaller with an increase in the K_m value ultimately plateauing at a concentration when the K_m value is the highest as the test concentrations are at non-saturating concentrations for P-gp.

Discussion

Although many drug transporters have been identified at the BBB, P-gp has been demonstrated to be the most important efflux transporter in limiting brain penetration of xenobiotics. The risk of developing a P-gp substrate as a CNS drug is the reduction of its

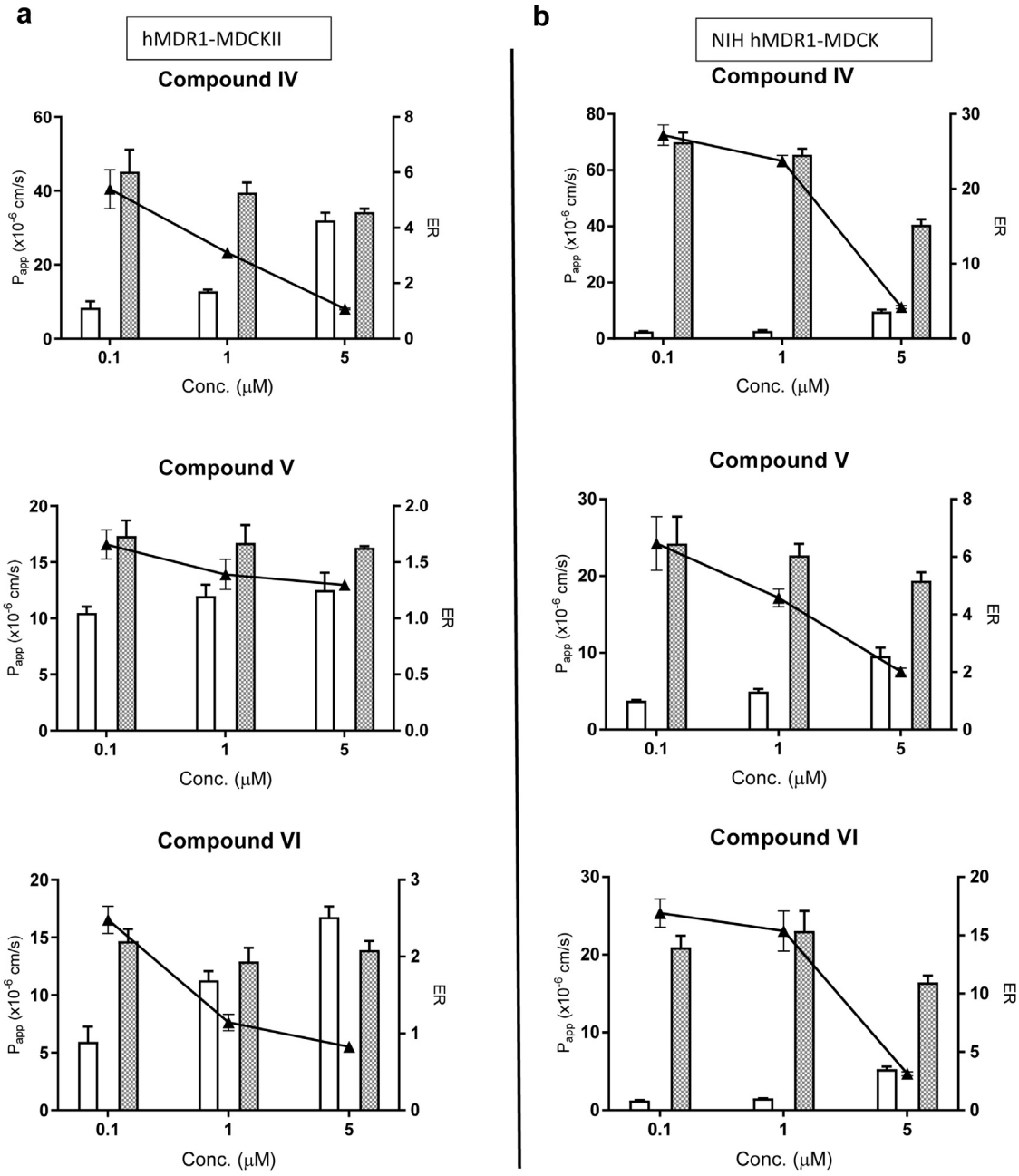

Fig. 4. (*continued*).

therapeutic window.[11] To achieve a sufficient coverage at the site of action within the CNS, a P-gp substrate requires a higher systemic exposure to compensate for the efflux activity at BBB, leading to increased risk of peripheral side-effects. A comprehensive evaluation of the 32 most prescribed CNS drugs indicated that the majority (>90%) of the drugs tested showed none or weak P-gp-mediated transport.[6] Therefore, a robust and reliable high-throughput P-gp efflux screening assay is necessary to support chemistry design and prioritization in order to triage strong P-gp substrates and identify the ideal candidate to be developed as CNS therapeutic. Rodent brain exposure data is typically used to confirm the findings of the validated P-gp assay. While this approach has been utilized broadly in the industry, the utility of the P-gp efflux assay has been limited to rank ordering compounds. The primary reason for this limitation is lack of consistency in data reported from different P-gp assays/cell lines, gaps in our understanding of the underlying reasons for such differences and specifications to identify a standard cell line. Although, the focus of this manuscript is related to utility of P-gp data and its correlation with CNS penetration, but it is a rather general issue related to the in vitro cell-based transporter models and not exclusive to P-gp. Traditional P-gp substrates used for assay validation have high Km values, so these differences across cell lines may have not been a significant issue in the past.

Recently, a significant disconnect was observed between P-gp efflux and brain penetration data generated for CNS discovery programs. Although, validated bidirectional P-gp efflux assay (using the hMDR1-MDCKII cell line generated with Flip-in™ technology) was being utilized, the P-gp ER data generated in vitro was not predictive of the brain exposure observed in rodents for

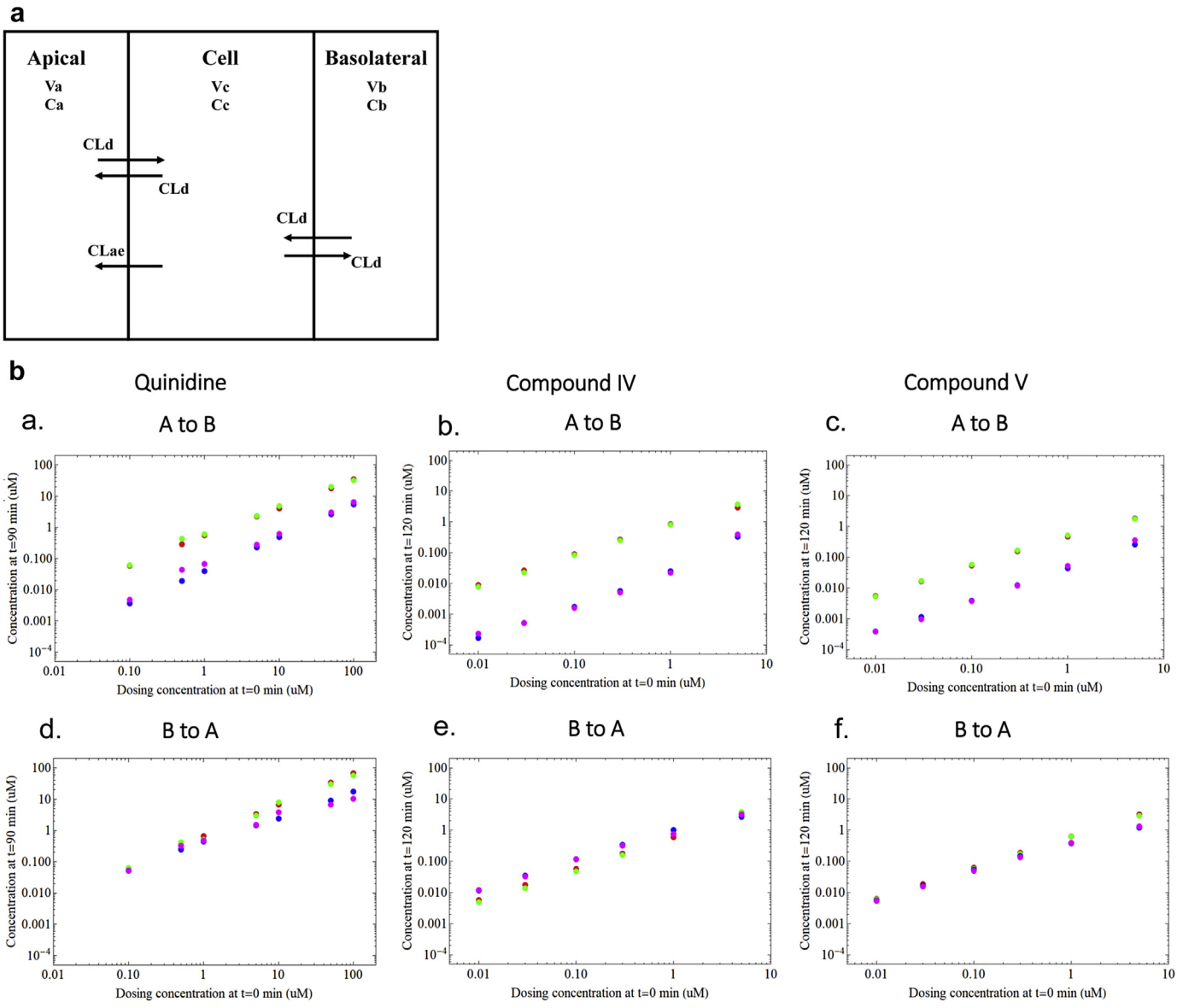

Fig. 5. Modeling of P-gp Kinetics. (A) 3-compartment (3-C) model including apical, cell and basolateral compartment. V_a, V_c, V_b denote the volumes of the apical, cellular and basolateral compartments; C_a, C_c and C_b denote the concentrations of the apical, cellular and basolateral compartments; CL_d is the passive diffusion clearance and CL_{ae} is the apical efflux clearance denoted by $\frac{V_{max}}{K_m+C_c}$. (B) Transporter data for quinidine, compound V and compound IV and their fitted data using 3-C model. P-gp efflux of quinidine were determined at a range of concentration (0.1 μM−100 μM) at 1.5-hr incubation in hMDR1-MDCK cell monolayer. P-gp efflux of Compound V and IV were determined at a range of concentration (0.01 μM−5 μM) at 2-hr incubation in TransFlex™ hMDR1-MDCKII cell monolayer. Panel a, b and c denote the substrate concentration in receiver and donor chambers from A to B experiments; Panels d, e and f denote the substrate concentration in receiver and donor chambers from B to A experiments; Experimental receiver and donor data are represented by magenta and green solid circles, respectively; Model predicted receiver and donor data are represented by blue and red circles, respectively.

compounds across multiple therapeutic targets. The poor brain penetration in rodents could be attributed to multiple factors including the involvement of other efflux transporters at BBB such as BCRP. Data (not shown) generated using human BCRP overexpressed MDCKII cell line suggested that BCRP could not account for the limited CNS exposure for these test articles. We further explored species differences in P-gp substrate specificity between human and rodent as a potential explanation for the observed disconnect. However, for the selected set of compounds, the P-gp efflux data from mMdr1a-MDCKII correlated well with those from NIH hMDR1-MDCK, suggesting minimal species difference in P-gp activity between mouse and human, consistent with previous findings.[9] However, based on the data, the possibility of the species difference in substrate specificity and affinity of test compounds with human and mouse P-gp cannot be completed ruled out. Finally, we tested P-gp saturation as the potential cause of false negative results in the previously validated hMDR1-MDCKII cell line; thus, leading to the disconnect between the ER and the brain penetration in rodents. By lowering the test concentrations in hMDR1-MDCKII, P-gp ER was significantly enhanced for most of the tested compounds, with exception of compound V and VI (ER < 3 at 0.1 μM) (Fig. 4). These data suggested that the dynamic range of hMDR1-MDCKII cell line was not able to fulfill the needs of the current chemical space being explored for the CNS discovery programs. Based on these observations, we decided to conduct a systematic study to explore various P-gp overexpressing cell lines for their suitability to be utilized for P-gp efflux assay. In the current study, four different P-gp cell lines were carefully characterized for

Table 1
P-gp Kinetic Parameter Estimates.

Compound	Quinidine	Compound IV	Compound V
Kinetic characterization from MDR1 MDCK Optivia cells			
Km (μM)	0.26 ± 0.05	0.05 ± 0.02	0.03 ± 0.01
Vmax (pmoles/min/cm^2)	12.14 ± 4.37	10.89 ± 2.64	3.06 ± 0.79
CL_d (μL/min/cm^2)	12.12 ± 1.46	9.61 ± 0.81	28.93 ± 1.52
$f_{u,cell}$	0.00092 ± 0.00022	0.00208 ± 0.00087	0.00027 ± 0.0003
3-Concentration assay in In-house MDR1 MDCK cells			
R_1	–	0.33 ± 0.07	0.22 ± 0.05
CLd (μL/min/cm^2)	–	11.08 ± 0.97	33.12 ± 1.17
3-Concentration assay in NIH MDR1 MDCK cells			
R_2	–	1.59 ± 0.20	1.25 ± 0.28
CLd (μL/min/cm^2)	–	10.39 ± 0.69	22.23 ± 1.86

R_1 represents the ratio of surface-active P-gp protein in TransFlex™ hMDR1-MDCKII versus hMDR1-MDCKII.
R_2 represents the ratio of surface-active P-gp protein in TransFlex™ hMDR1-MDCKII versus NIH hMDR1-MDCK.

P-gp expression and localization, compared for P-gp efflux activity and the predictability of brain penetration. A set of compounds with P-gp ER lower than 3 determined in hMDR1-MDCKII were selected from CNS discovery programs as a training set to evaluate P-gp efflux activity among the selected cell lines. The data in Fig. 2 demonstrated the P-gp liabilities for 12 compounds were confirmed in the mouse Mdr1a cell line and 30 compounds were confirmed in NIH MDR1 cell line. The P-gp ER determined in NIH MDR1 cell line demonstrate the most robust correlation with brain penetration data (Kp_{uu}) in rodent, followed by mouse Mdr1a cells (Fig. 3). This finding is aligned with previous work demonstrating that P-gp ER in NIH-MDR1 cell line can better predict in vivo brain penetration in rodents, compared to another widely used MDR1 cell line from Borst Lab, The Netherlands with much lower P-gp expression compared to NIH MDR1 cell line.[7,13]

Based on the assumption that total amount of transporter protein correlates to the efflux activity, it is speculated that the superior activity of NIH MDR1 cell line may be attributed to the higher expression level of P-gp protein. To test the hypothesis, the P-gp protein expressed in the different cell lines tested in the study were

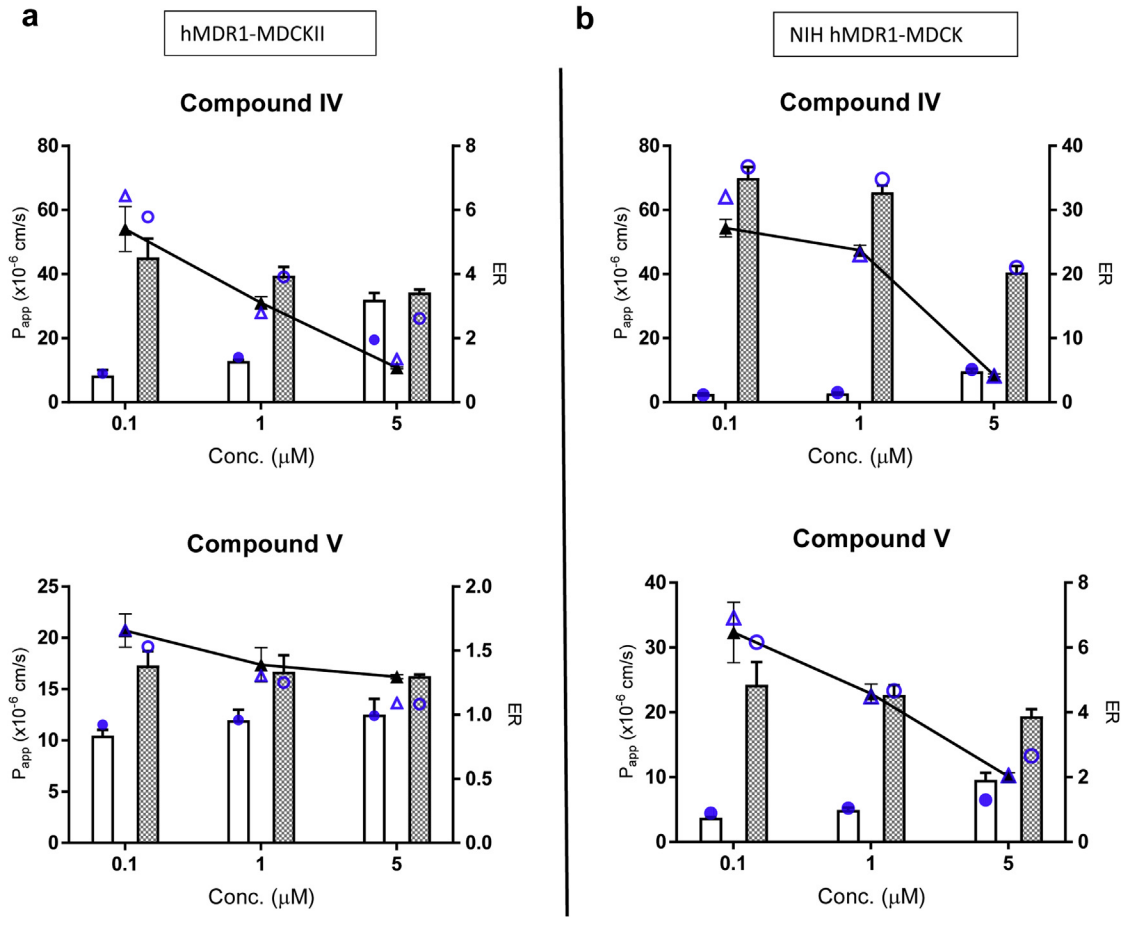

Fig. 6. Prediction of P-gp efflux of Compound IV and V in hMDR1-MDCKII (A) and NIH hMDR1-MDCK (B) using 3-C modeling with fixed system-independent K_m values. Open bar: observed $P_{app\ A>B}$; patterned bar: observed $P_{app\ B>A}$; solid triangle: observed ER; blue solid circle: predicted $P_{app\ A>B}$; blue open circle: predicted $P_{app\ B>A}$; blue open triangle: predicted ER.

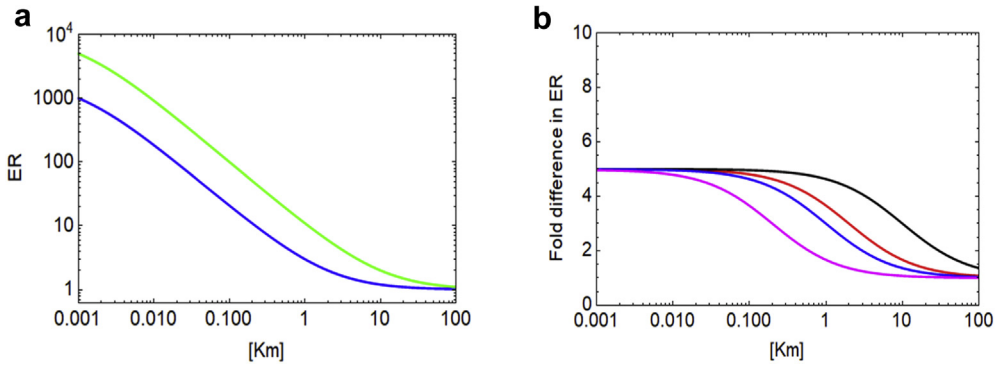

Fig. 7. Simulation of the impact of system-independent Km on P-gp ER in cell lines with differential P-gp expression level. (A) Effect of Km on efflux ratio at Vmax = 1 μL/min (Blue) and 5 μL/min (Green) representing the 5-fold difference of P-gp expression level. (B) Fold change in ER at range of CLd = 0.1 μL/min (Black), 0.5 μL/min (Red), 1 μL/min (Blue) and 5 μL/min (Magenta), where fold change is defined as (ER at Vmax = 5 μL/min)/(ER at Vmax = 1 μL/min).

carefully characterized using quantitative proteomics (Fig. 1A). It was observed that P-gp protein expression was at least 10-fold higher in NIH hMDR1-MDCK compared to hMDR1-MDCKII, which can explain the significantly improved P-gp substrate identification and largely improved correlation with rodent brain penetration data in vivo. In addition, confocal imaging analysis of immunostained P-gp in these two MDR1 cell lines further confirmed that nearly all of the P-gp protein was localized on the plasma membrane in NIH hMDR1-MDCK (Fig. 1B). In contrast, the P-gp protein in hMDR1-MDCKII was expressed at much lower levels and significant portion of it was found in intracellular compartments in addition to plasma membrane (Fig. 1B), indicating the marked difference in P-gp trafficking pattern between the two cell lines. These results suggested that the difference in absolute cell surface P-gp expression between the two human MDR1 cell lines is much larger than the difference observed in the total crude membrane fraction based on quantitative proteomic data. Hence, it was not possible to use the quantitative proteomic data to model P-gp kinetics in this study since the active membrane transporter protein could not be quantified.

The results from the protein expression analysis were also corroborated by the surface-active P-gp fold-difference in these cell lines, which were estimated using compartmental modeling (Table 1). The ratio of P-gp protein abundance in hMDR1-MDCKII and TransFlex™ hMDR1-MDCKII was 0.3 as determined by targeted proteomics, which aligned well with the estimated surface-active P-gp ratio (0.22 and 0.33) between these two cell lines when assessed by compartmental modeling. However, the estimated surface-active P-gp ratio (1.25 and 1.59) between NIH hMDR1-MDCK and TransFlex™ hMDR1-MDCKII was lower than the ratio of P-gp protein abundance (7.3) determined using targeted proteomics. The difference could be attributed to several factors including the presence of nonfunctional P-gp protein on the plasma membrane, intracellular depots of P-gp protein[31] or not all functional P-gp contributing to transport due to futile cycling.[32]

The concentration-dependent efflux assessment in NIH hMDR1-MDCK cell line further demonstrated the phenomena of differential P-gp saturation. In contrast to hMDR1-MDCKII, P-gp ER for all the tested compounds was greater than 3 at 1.0 μM in NIH hMDR1-MDCK cell lines. These results suggest that the apparent P-gp K_m was different between hMDR1-MDCKII and NIH hMDR1-MDCK. In classic enzyme kinetic experiments, a direct Michaelis-Menten analysis of the data may be appropriate since the incubation concentration is the driving concentration for these reactions. As is increasingly evident from recent literature, direct Michaelis-Menten analysis of bidirectional P-gp efflux assays does not yield a 'true' K_m of a compound but instead gives an 'apparent' K_m which is dependent on the P-gp protein expression level; higher expression resulting in a greater apparent K_m.[33] These differences may not be limited to K_m values but are likely to extend to other kinetic parameters. Large inter-laboratory variability observed in P-gp IC_{50} values across 23 different laboratories, using various routinely used P-gp cell lines and membrane vesicles, may be explained in part by differences in P-gp expression level.[12]

The bidirectional P-gp efflux assay, consists of multiple compartments, where P-gp substrate first has to cross the plasma membrane and enter the cellular compartment through passive diffusion and/or active uptake, followed by interaction with the P-gp protein before being pumped out to the apical compartment. Thus, compartmental modeling of data from bidirectional efflux assays has resulted in a more consistent estimation of the K_m from different cell systems with varied P-gp expression levels across laboratories.[16,22] The K_m determined by compartmental modeling for quinidine in our study was also in agreement with the reported value[22] giving us confidence in our approach. Thus, it is the system independent K_m which is a measure of the inherent affinity of a compound towards P-gp and should be used for in vitro to in vivo correlation when predicting brain penetration. Physiologically based pharmacokinetic (PBPK) models have been explored to predict the effect of P-gp on brain penetration in human.[34,35] It is important to use the system-independent kinetic parameters when conducted such analysis.

Further, it was hypothesized that the current chemical space in CNS discovery has shifted in term of the P-gp binding affinity with much lower system independent K_m. Hence, lowering the test concentration from 5 to 0.1 μM resulted in a higher ER in both hMDR1-MDCKII and NIH hMDR1-MDCK cell lines. Indeed, the K_m estimated from compartmental modeling of Comp V and Comp IV were very low (0.03 and 0.05 μM, respectively). It is noteworthy that the fold change in ER between these two MDR1 cell lines is different for different compounds. Simulation results suggested that the extent of the impact of protein expression level on P-gp ER is dependent on the inherent system-independent K_m and the passive diffusion clearance relative to active efflux clearance of the test article. The impact is more drastic for the compounds with low system-independent K_m compared to the ones with high system-independent K_m. For compounds with similar K_m values, a lower passive diffusion clearance likely leads to more pronounced difference in observed ER in the cell lines with different P-gp expression levels (Fig. 7). The net effect of these factors will govern the extent of the change in P-gp ER as is seen from the analysis of Compound V (K_m = 0.03 μM, CL_d 28.93 μL/min) and Compound IV

($K_m = 0.05$ μM, CL_d 9.61 μL/min) demonstrating an ER fold change of 3.4 and 5 at concentration of 0.1 μM in NIH hMDR1-MDCK and hMDR1-MDCKII respectively. Therefore, the fold change in ER in cell lines with different P-gp expression levels should be interpreted with caution since ER is a complex function of the V_{max}, K_m and passive diffusion clearance (CL_d).

In conclusion, through the comprehensive characterization of a variety of P-gp cell lines, we found that the discrepancies in P-gp ER between different cell lines can be explained by the differential P-gp expression levels. Using modeling and simulation approach, system-independent P-gp K_m values were determined and demonstrated to predict the P-gp efflux activity in cell lines with different P-gp expression levels. As the chemical space in CNS discovery is continuously evolving, attention should be paid to the characterization of in vitro P-gp assays in order to predict brain penetration with confidence. Although the current study focused on explaining the discrepancy observed in P-gp substrate assessment for CNS therapeutics, these challenges would be independent of any specific therapeutic area. Appropriate assessment of drug interaction with P-gp as a substrate and/or inhibitor is especially critical for drug-drug interaction assessment. Careful introspection of in vitro P-gp models is critical for employing them at various stages of drug discovery and development.

Acknowledgements

Authors would like to acknowledge John Roberts for providing binding parameters. Authors would also like to thank Dan Rock, Jan Wahlstrom, and Dean Hickman for their support of this work.

Appendix A. Supplementary Data

Supplementary data to this article can be found online at https://doi.org/10.1016/j.xphs.2020.09.017.

References

1. Pardridge WM. Blood-brain barrier biology and methodology. *J Neurovirol*. 1999;5(6):556-569.
2. Zhang Y, Li N, Brown PW, Ozer JS, Lai Y. Liquid chromatography/tandem mass spectrometry based targeted proteomics quantification of P-glycoprotein in various biological samples. *Rapid Commun Mass Spectrom*. 2011;25(12):1715-1724.
3. Schinkel AH. P-Glycoprotein, a gatekeeper in the blood-brain barrier. *Adv Drug Deliv Rev*. 1999;36(2-3):179-194.
4. Schinkel AH, Smit JJ, van Tellingen O, et al. Disruption of the mouse mdr1a P-glycoprotein gene leads to a deficiency in the blood-brain barrier and to increased sensitivity to drugs. *Cell*. 1994;77(4):491-502.
5. Kusuhara H, Sugiyama Y. Active efflux across the blood-brain barrier: role of the solute carrier family. *NeuroRx*. 2005;2(1):73-85.
6. Doran A, Obach RS, Smith BJ, et al. The impact of P-glycoprotein on the disposition of drugs targeted for indications of the central nervous system: evaluation using the MDR1A/1B knockout mouse model. *Drug Metab Dispos*. 2005;33(1):165-174.
7. Kikuchi R, de Morais SM, Kalvass JC. In vitro P-glycoprotein efflux ratio can predict the in vivo brain penetration regardless of biopharmaceutics drug disposition classification system class. *Drug Metab Dispos*. 2013;41(12):2012-2017.
8. Mahar Doan KM, Humphreys JE, Webster LO, et al. Passive permeability and P-glycoprotein-mediated efflux differentiate central nervous system (CNS) and non-CNS marketed drugs. *J Pharmacol Exp Ther*. 2002;303(3):1029-1037.
9. Feng B, Mills JB, Davidson RE, et al. In vitro P-glycoprotein assays to predict the in vivo interactions of P-glycoprotein with drugs in the central nervous system. *Drug Metab Dispos*. 2008;36(2):268-275.
10. Polli JW, Wring SA, Humphreys JE, et al. Rational use of in vitro P-glycoprotein assays in drug discovery. *J Pharmacol Exp Ther*. 2001;299(2):620-628.
11. Liu X, Chen C, Smith BJ. Progress in brain penetration evaluation in drug discovery and development. *J Pharm Exp Ther*. 2008;325(2):349-356.
12. Bentz J, O'Connor MP, Bednarczyk D, et al. Variability in P-glycoprotein inhibitory potency (IC(5)(0)) using various in vitro experimental systems: implications for universal digoxin drug-drug interaction risk assessment decision criteria. *Drug Metab Dispos*. 2013;41(7):1347-1366.
13. Feng B, West M, Patel NC, et al. Validation of human MDR1-MDCK and BCRP-MDCK cell lines to improve the prediction of brain penetration. *J Pharm Sci*. 2019;108(7):2476-2483.
14. Bentz J, Tran TT, Polli JW, Ayrton A, Ellens H. The steady-state Michaelis-Menten analysis of P-glycoprotein mediated transport through a confluent cell monolayer cannot predict the correct Michaelis constant Km. *Pharm Res (N Y)*. 2005;22(10):1667-1677.
15. Korzekwa K, Nagar S. Compartmental models for apical efflux by P-glycoprotein: part 2–a theoretical study on transporter kinetic parameters. *Pharm Res (N Y)*. 2014;31(2):335-346.
16. Tachibana T, Kitamura S, Kato M, et al. Model analysis of the concentration-dependent permeability of P-gp substrates. *Pharm Res (N Y)*. 2010;27(3):442-446.
17. Heikkinen AT, Korjamo T, Lepikko V, Monkkonen J. Effects of experimental setup on the apparent concentration dependency of active efflux transport in in vitro cell permeation experiments. *Mol Pharm*. 2010;7(2):605-617.
18. Meng Z, Ellens H, Bentz J. Extrapolation of elementary rate constants of P-glycoprotein-Mediated transport from MDCKII-hMDR1-NKI to caco-2 cells. *Drug Metab Dispos*. 2017;45(2):190-197.
19. Zamek-Gliszczynski MJ, Lee CA, Poirier A, et al. ITC recommendations for transporter kinetic parameter estimation and translational modeling of transport-mediated PK and DDIs in humans. *Clin Pharmacol Ther*. 2013;94(1):64-79.
20. Xu M, Saxena N, Vrana M, et al. Targeted LC-MS/MS proteomics-based strategy to characterize in vitro models used in drug metabolism and transport studies. *Anal Chem*. 2018;90(20):11873-11882.
21. Basit A, Radi Z, Vaidya VS, Karasu M, Prasad B. Kidney cortical transporter expression across species using quantitative proteomics. *Drug Metab Dispos*. 2019;47(8):802-808.
22. Korzekwa KR, Nagar S, Tucker J, Weiskircher EA, Bhoopathy S, Hidalgo IJ. Models to predict unbound intracellular drug concentrations in the presence of transporters. *Drug Metab Dispos*. 2012;40(5):865-876.
23. Nakai D, Kumamoto K, Sakikawa C, Kosaka T, Tokui T. Evaluation of the protein binding ratio of drugs by a micro-scale ultracentrifugation method. *J Pharm Sci*. 2004;93(4):847-854.
24. Nagahara N, Tavelin S, Artursson P. Contribution of the Paracellular Route to the pH-dependent epithelial permeability to cationic drugs. *J Pharm Sci*. 2004;93(12):2972-2984.
25. Pade V, Stavchansky S. Estimation of the relative contribution of the transcellular and paracellular pathway to the transport of passively absorbed drugs in the Caco-2 cell culture model. *Pharm Res*. 1997;14(9):1210-1215.
26. Sugano K, Takata N, Machida M, Saitoh K, Terada K. Prediction of passive intestinal absorption using bio-mimetic artificial membrane permeation assay and the paracellular pathway model. *Int J Pharm*. 2002;241(2):241-251.
27. Li N, Nemirovskiy OV, Zhang Y, et al. Absolute quantification of multidrug resistance-associated protein 2 (MRP2/ABCC2) using liquid chromatography tandem mass spectrometry. *Anal Biochem*. 2008;380(2):211-222.
28. Kamiie J, Ohtsuki S, Iwase R, et al. Quantitative atlas of membrane transporter proteins: development and application of a highly sensitive simultaneous LC/MS/MS method combined with novel in-silico peptide selection criteria. *Pharm Res (N Y)*. 2008;25(6):1469-1483.
29. Broccatelli F, Larregieu CA, Cruciani G, Oprea TI, Benet LZ. Improving the prediction of the brain disposition for orally administered drugs using BDDCS. *Adv Drug Deliv Rev*. 2012;64(1):95-109.
30. Kalvass JC, Maurer TS, Pollack GM. Use of plasma and brain unbound fractions to assess the extent of brain distribution of 34 drugs: comparison of unbound concentration ratios to in vivo p-glycoprotein efflux ratios. *Drug Metab Dispos*. 2007;35(4):660-666.
31. Kumar V, Salphati L, Hop C, et al. A comparison of total and plasma membrane abundance of transporters in suspended, plated, sandwich-cultured human hepatocytes versus human liver tissue using quantitative targeted proteomics and cell surface biotinylation. *Drug Metab Dispos*. 2019;47(4):350-357.
32. Meng Z, Le Marchand S, Agnani D, Szapacs M, Ellens H, Bentz J. Microvilli morphology can affect efflux active P-glycoprotein in confluent MDCKII-hMDR1-NKI and caco-2 cell monolayers. *Drug Metab Dispos*. 2017;45(2):145-151.
33. Shirasaka Y, Sakane T, Yamashita S. Effect of P-glycoprotein expression levels on the concentration-dependent permeability of drugs to the cell membrane. *J Pharm Sci*. 2008;97(1):553-565.
34. Trapa PE, Troutman MD, Lau TY, et al. In vitro-in vivo extrapolation of key transporter activity at the blood-brain barrier. *Drug Metab Dispos*. 2019;47(4):405-411.
35. Trapa PE, Belova E, Liras JL, Scott DO, Steyn SJ. Insights from an integrated physiologically based pharmacokinetic model for brain penetration. *J Pharm Sci*. 2016;105(2):965-971.